arXiv:1403.5157v1 [cond-mat.mtrl-sci] 20 Mar 2014

Magnetization of densely packed interacting magnetic nanoparticles with cubic and uniaxial anisotropies: a Monte Carlo study.

V. Russier [a], C. de-Montferrand [b], Y. Lalatonne [b] and L. Motte [b].

[a] *ICMPE, UMR 7182 CNRS and UPEC, 2-8 rue Henri Dunant 94320 Thiais, France. and*

[b] *CSPBAT UMR 7244 CNRS and University Paris 13, 93017 Bobigny, France.*

(Dated: February 28, 2022)

The magnetization curves of densely packed single domain magnetic nanoparticles (MNP) are investigated by Monte Carlo simulations in the framework of an effective one spin model. The particles whose size polydispersity is taken into account are arranged in spherical clusters and both dipole dipole interactions (DDI) and magnetic anisotropy energy (MAE) are included in the total energy. Having in mind the special case of spinel ferrites of intrinsic cubic symmetry, combined cubic and uniaxial magnetocrystalline anisotropies are considered with different configurations for the orientations of the cubic and uniaxial axes. It is found that the DDI, together with a marked reduction of the linear susceptibility are responsible for a damping of the peculiarities due to the MAE cubic component on the magnetization. As an application, we show that the simulated magnetization curves compare well to experimental results for γ–Fe_2O_3 MNP for small to moderate values of the field.

I. INTRODUCTION

Magnetic nanoparticles (MNP) assemblies present a fundamental interest in the development of nanoscale magnetism research and are promising candidates in a wide range of potential applications going from high density recording to bio-medicine[1–5]. Experimentally MNP can be obtained either as colloidal suspensions where the concentration can be varied at will, embedded in non magnetic material where one can tune the interparticle interactions or as powder samples where they form densely packed systems. The case of iron oxide particles, which are typical cubic spinel ferrites take a central place especially for bio-medical applications because of their biocompatibility and suitable superparamagnetic properties[6,7].

The magnetic behavior of nanostructured materials or systems including nanoscale magnetic particles is a multiscale problem since the local magnetic structure within NP at the atomic site scale presents non trivial features[8–11] and the interactions between particles play an important role. A simplification occurs for NP of diameter below some critical value of typically few tens of nanometers since they then reach the single domain regime and can be described through an effective one spin model (EOS) where each NP is characterized by its moment and anisotropy energy. However both the moment value

and the anisotropy energy function are to be understood as effective quantities which take into account some of the atomic scale characteristics[12–15]. The EOS type of approach is a simplifying but necessary step for the description of interacting MNP assemblies. In the framework of the EOS models, the total energy includes on the one hand the NP anisotropy energy through a one-body term and on the other hand the interparticle interactions. It is generally assumed for frozen systems of well separated NP that the leading term in the interparticle interactions is the dipolar interaction (DDI) between the macrospins which is totally determined once the NP saturation magnetization and the size distribution are known. Conversely modeling the anisotropy energy is not straightforward since in finite sized particles it comes from different origins. The intrinsic contribution which stems form the bulk material is *a priori* known experimentally without ambiguity. It can be of either uniaxial or cubic symmetry according to the crystalline structure with anisotropy constants whose magnitude and even sign depend on temperature. In the widely studied case of oxide spinel ferrites at room temperature the intrinsic anisotropy is of cubic symmetry[16–20] with in general a negative constant K_c, leading to the moment preferentially oriented along the $\{111\}$ directions of the crystallites. Then for NP not strictly spherical one has to add the shape anisotropy term resulting from demagnetizing effect at the particle scale which for ellipsoidal NP is uniaxial with a shape anisotropy constant proportional to the NP volume[1]. Finally the finite size of the NP is the source of surface anisotropy resulting from symmetry breaking, surface defects or chemical bonding of the coating layer. When modeled by a transverse anisotropy or the Néel surface anisotropy model[21], the resulting non collinearities of the surface spins can be represented through a cubic term in the framework of the EOS[14,15]. Concerning spherical iron oxide nanoparticles, the general experimental observation is that the uniaxial anisotropy dominates with however a rather large dispersion in the effective annisotropy constant value K_{eff}[13,22–27]. Moreover a small value of K_{eff} is interpreted as a small amount of crystalline defects within or at the nanoparticle surface[24,27–29]. In any case the effective uniaxial anisotropy constant cannot be compared to the intrinsic, or bulk one, since the latter corresponds to the cubic symmetry and is negative at room temperature. Furthermore from the particle size dependence it is generally concluded that the uniaxial anisotropy is predominantly a surface anisotropy with a related constant $K_s = (d/6)K_{eff}$[13,22,26].

At the atomic scale the well known Néel model of pair anisotropy[21] is often invoked to deduce surface anisotropy either in thin film geometry or in 3D NP. In the framework of EOS approach, the deviation from the spherical shape translates in the Néel pair anisotropy model, in addition to the magnetic dipolar term responsible for the shape anisotropy, in a contribution with the same symmetry and proportional to the NP surface because of its short range character. This leads for ellipsoidal NP to a surface contribution of uniaxial

symmetry. One has to keep in mind however that the Néel model although useful in the sense that it reproduces the correct description of the symmetry of the magnetic anisotropy, does not provide the physical understanding of the single ion anisotropy[30]. Thus when dealing with spinel ferrites oxides as well as with Fe or Ni single domain nearly spherical nanoparticles in the framework of a EOS model, combined uniaxial and cubic anisotropies should be taken into account because of the intrinsic cubic anisotropy on the one hand, the shape (uniaxial) and surface contributions (uniaxial and/or cubic) on the other hand.

In Ref. [31] the expansion of the linear and non linear susceptibility for non interacting assembly with either uniaxial or cubic anisotropy has been performed with the result that when the 3 axes of the cubic contribution are randomly distributed both the linear and the first non linear susceptibilities are anisotropy independent. In Ref. [32] the LLG equation is considered to calculate the hysteresis curve at vanishing temperature of non interacting NP, with randomly oriented cubic axes. The easy axis of the uniaxial term is either fixed at conveniently chosen direction or randomly distributed. In Ref. [33] an assembly of weakly interacting NP is considered both from perturbation theory and MC simulations with cubic anisotropy relative to the same cubic axes for all the NP combined with an uniaxial anisotropy with a random distribution of easy axes.

In the present work, we perform MC simulation of NP assemblies interacting through DDI with cubic and uniaxial contributions to the anisotropy energy. Having in mind the case of strongly interacting powder samples of NP dispersed at zero field, we consider the case of NP with cubic axes randomly distributed. The uniaxial easy axis on the other hand is either randomly distributed independently of the cubic axes or oriented along a particular crystallographic orientation of the particles for which two cases are considered, namely {100} or {111}. The main purpose of the present work is to investigate whether the cubic contribution to the anisotropy leads to an observable deviation to the magnetization curve in the superparamagnetic regime. We also revisit the consequences of the DDI in the strong coupling regime, in particular on the linear susceptibility at low field, through the comparison of simulations performed either with free boundary conditions on spherical cluster or with periodic boundary conditions to simulate an infinite system.

In section II, we give the details of the model and explicit the different energy contributions. Section III is devoted to the results and the comparison with experimental results and we briefly conclude in section IV.

II. MODEL FOR DENSELY PACKED ASSEMBLIES

We consider a EOS model with nanoparticles described as non overlapping spheres bearing at their center a permanent point dipole representing the uniform magnetization of the particle (macro spin). The moment of each particle is equal to its volume times the bulk magnetization, M_s, which means that no spin canting effect is explicitly taken into account. The particles are surrounded by a non magnetic layer of thickness $\Delta/2$, representing the usual coating by organic surfactant molecules. The particle diameters, $\{d_i\}$ are distributed according to a log-normal law defined by the median diameter d_m and the standard deviation σ of $ln(d)$,

$$f(d) = \frac{1}{d\sqrt{2\pi}\sigma} \exp\left(-\frac{(\ln(d/d_m))^2}{2\sigma^2}\right) \tag{1}$$

In the following, we use d_m as the unit of length, and the distribution function in reduced unit is totally determined by the single parameter σ which characterizes the system polydispersity. When dealing with interacting particles, we mainly have in mind the case of lyophilized powders samples or high concentration nanoparticles assemblies embedded in non magnetic matrix. Accordingly the coated particles are distributed in densely packed clusters whose external shape is spherical in order to avoid the demagnetizing effects due to the system shape with the free boundary conditions. We emphasize that this NP configuration has an experimental justification since upon drying the NP are likely to aggregate in spherical shaped large clusters which has been confirmed from simulations[34]. Moreover, we consider mainly the superparamagnetic regime, where we simulate only equilibrium magnetization curves corresponding to the static or infinite time measurements ($\tau_m \ \rightarrow \ \infty$).

We include only the leading terms of the anisotropy energy; the cubic symmetry contribution for particle say i of moment $v(d_i)M_s\hat{m}_i$ can be written as

$$\frac{E_c^{(i)}}{v(d_i)} = K_c\left(m_{xi}^2 m_{yi}^2 + m_{yi}^2 m_{zi}^2 + m_{xi}^2 m_{zi}^2\right) = \frac{K_c}{2}\left(1 - \sum_{\alpha=x,y,z} m_{\alpha i}^4\right) \tag{2}$$

where we have used the unitarity of $\hat{m}_i$ in the second equality. Here and in the following hated letters denote unit vectors. In equation (2) $m_{\alpha i}$ refer to the $\hat{m}_i$ components in the local cubic frame of the particle considered. Let us denote by $\{\hat{x}_{\alpha i}\}, \alpha = 1,3$ this local cubic frame; dropping an irrelevant constant, the total cubic anisotropy of the system can be written

$$E_c = -\frac{K_c}{2}\sum_i v(d_i)\sum_\alpha (\hat{x}_{\alpha i}\hat{m}_i)^4 \tag{3}$$

The local axes $\{\hat{x}_{\alpha i}\}$ can be oriented in different ways according to the physical system under study; for non textured distributions of particles we have to consider a random distribution of the $\{\hat{x}_{\alpha i}\}$. Most of our simulations are performed in the case. The effect of the texturation is nevertheless examined by considering that the [111] directions $\{\hat{x}_1+\hat{x}_2+\hat{x}_3\}_i$ or the $\{\hat{x}_3\}_i$ axes are confined in a cone along the $\hat{z}$-axis according to the following probability distribution for polar angles

$$P(\theta) = Csin(\theta)exp(-(\theta/\sigma_\theta)^2/2) \ ; \tag{4}$$

The configuration with the $\{\hat{x}_{\alpha i}\}$ fixed parallel to the system frame $(\hat{x}, \hat{y}, \hat{z})$ is also considered. This later case is the same as that Margaris et al.[33] considered for which a strong effect of the cubic term is obtained while Usov and Barandiarán[32] consider cubic axes randomly distributed. Although we have in mind particles of intrinsic cubic anisotropy, we are aware of a possible surface contribution to E_c as shown in Ref. [14] resulting from the non collinearity of the surface spins; as a result the value of K_c may differ form the bulk one. The uniaxial term is proportional either to the volume $v(d)$ or to the surface $s(d)$ of the particle. The volume part stems *a priori* from the shape anisotropy where for ellipsoidal particles $K_{sh}^{(u)}$, given by $J_s^2(1-3N_u)/(4\mu_0)$ with $J_s = \mu_0 M_s$ and N_u, the demagnetizing factor along the revolution axis, can be deduced from the knowledge of the aspect ratio ξ. Notice that one can imagine easily a situation where the deviation from sphericity is not characterized by the same aspect ratio for all particles leading to a size dependence of K_{sh}. For instance one cannot rule out the situation where the deviation from sphericity follows from a major axis of the form $c = (d/2 + \delta)$ and minor axes $a = b = d/2$, with a size independent corrugation δ. Then from the demagnetizing factor in the major axis direction

$$N_u = \frac{1-\epsilon^2}{2\epsilon^3}\left[\ln\left(\frac{1+\epsilon}{1-\epsilon}\right) - 2\epsilon\right] \quad ; \quad \text{with} \quad \epsilon = (1-1/\xi^2)^{1/2} \quad \text{and} \quad \xi = c/a = 1 + 2\delta/d \ ,$$

the shape anisotropy may transform in a surface uniaxial anisotropy with an anisotropy constant given by $K_s^{(u)} \simeq J_s^2\delta/(30\mu_0)$ from an expansion of $K_{sh}^{(u)}$ at order δ/d.

The easy axes $\{\hat{n}\}_i$ are either randomly distributed independently of the particles frame or aligned along one specified crystallographic axis of the crystallite. Different origin for such a easy axes distribution can be invoked. In the framework of the uniaxial anisotropy originating from the deviation to sphericity it corresponds to a preferential crystallographic orientation for crystallite growth, while in the framework of the uniaxial surface anisotropy this may result from a preferential crystallographic orientation for chemical bonding at the particle surface. We have considered two possibilities, namely $\hat{n}_i = \{001\}_i$ or $\hat{n}_i = \{111\}_i$.

In the total energy, we include formally both surface and volume terms in the uniaxial

contribution, with anisotropy constants $K_v^{(u)}$ and $K_s^{(u)}$ respectively and at most one of these is non zero in the simulations. The total energy thus includes the DDI, the one-body anisotropy term and the Zeeman term corresponding to the interaction with the external applied field $\vec{H}_a = H_a\hat{h}$. Let $\{\vec{r}_i\}$, $\{v(i)\}$, $\{\vec{m}_i\}$ and $\{\vec{n}_i\}$ denote the particles locations, volumes, moments and easy axes respectively. The total energy of the cluster reads

$$E = \frac{\mu_0}{4\pi}\sum_{i<j} m_i m_j \frac{\hat{m}_i\hat{m}_j - 3(\hat{m}_i\hat{r}_{ij})(\hat{m}_j\hat{r}_{ij})}{r_{ij}^3} - \sum_i (K_v^{(u)}v(i) + K_s^{(u)}s(i))(\hat{n}_i\hat{m}_i)^2 - \frac{K_c}{2}\sum_i v(i)\sum_\alpha (\hat{m}_i\hat{x}_{\alpha i})^4 - \mu_0 H_a \sum_i m_i\hat{m}_i\hat{h} \quad (5)$$

m_i are the moment magnitudes, $r_{ij} = |\vec{r}_i - \vec{r}_j|$. It is worth mentioning that the consideration of the anisotropy term with a fixed easy axes distribution means that the magnetization relax according to a Néel process[16,35], namely the particles are considered fixed while their moment relaxes relative to their easy axis. In the following we use reduced quantities; first the energy is written in k_BT_0 units, T_0 being a suitable temperature ($T_0 = 300K$ in the present work) and we introduce a reference diameter, d_{ref}. The reference diameter, d_{ref} is a length unit independent of the size distribution, useful for the energy couplings, and can be chosen from a convenient criterion independently of the actual structure of the MNP assembly. The reduced total energy is given by

$$\begin{aligned}\beta_0 E \;=\; & -\epsilon_{uv}^{(0)}\left(\frac{d_m}{d_{ref}}\right)^3 \sum_i d_i^{*3}(\hat{n}_i\hat{m}_i)^2 - \epsilon_{us}^{(0)}\left(\frac{d_m}{d_{ref}}\right)^2 \sum_i d_i^{*2}(\hat{n}_i\hat{m}_i)^2 \\ & - \frac{\epsilon_c^{(0)}}{2}\left(\frac{d_m}{d_{ref}}\right)^3 \sum_i d_i^{*3}\sum_\alpha (\hat{m}_i\hat{x}_{\alpha i})^4 - \epsilon_d^{(0)}\left(\frac{d_m}{d_{ref}}\right)^3 \sum_{i<j} d_i^{*3}d_j^{*3}\frac{\hat{m}_i\hat{m}_j - 3(\hat{m}_i\hat{r}_{ij})(\hat{m}_j\hat{r}_{ij})}{r_{ij}^{*3}} \\ & - h\sum_i d_i^{*3}\hat{m}_i\hat{h}\ , \end{aligned} \quad (6)$$

with

$$\epsilon_{uv}^{(0)} = \beta_0 K_v^{(u)} v(d_{ref})\ ;\ \epsilon_{us}^{(0)} = \beta_0 K_s^{(u)} s(d_{ref})\ ;\ \epsilon_c^{(0)} = \beta_0 K_c v(d_{ref})$$
$$\epsilon_d^{(0)} = \frac{\beta_0\mu_0}{4\pi}(\pi/6)^2 M_s^2 d_{ref}^3\ ;\ h = \beta_0\mu_0 M_s(\pi/6)d_m^3 H_a \equiv \left(\frac{d_m}{d_{ref}}\right)^3 \frac{H_a}{H_{ref}} \quad (7)$$

where $\beta_0 = (k_BT_0)^{-1}$ and the stared lengths are in d_m unit. The dimensionless dipolar coupling constant is then $\epsilon_d = (d_m/d_{ref})^3\epsilon_d^{(0)}$ and the dimensionless anisotropy constants are $\epsilon_{uv} = (d_m/d_{ref})^3\epsilon_{uv}^{(0)}$, $\epsilon_{us} = (d_m/d_{ref})^2\epsilon_{us}^{(0)}$, and $\epsilon_c = (d_m/d_{ref})^3\epsilon_c^{(0)}$ for the volume and surface uniaxial and cubic contributions respectively. The reference diameter, d_{ref} can be chosen such that $\epsilon_d(d_m = d_{ref}) \equiv \epsilon_d^{(0)} = 1$; the reduced external field h coincides with the usual Langevin variable at temperature T_0 for a monodisperse distribution with $d = d_m$

In equation (7), we also introduce the reference external field, H_{ref} for convenience.

Concerning the structure in position, the nanoparticles surrounded by their coating layer of thickness $\Delta/2$ form an assembly of hard spheres of effective diameters $\{d_i + \Delta\}$ which are arranged in large densely packed clusters with either a random or a well ordered simple structure (simple cubic lattice) The clusters are built as in Ref. [36]. First a large stacking of the coated spheres is made in a parallepipedic box with the desired structure, random or well ordered. Once this first step is performed, we cut within the global stacking the cluster we want to study by imposing both the external shape and the number of particles N_p, with typically $N_p \simeq 1000$. Because of the coating layer of thickness $\Delta/2$ the closest distance of approach between particles i, j is shifted from $(d_i + d_j)/2$ to $(d_i + d_j)/2 + \Delta$ and we therefore define an effective dipolar constant corresponding the particles uncoated at contact

$$\epsilon_d^{eff} = \epsilon_d \frac{1}{(1 + \Delta/d_m)^3} = \epsilon_d \frac{\phi}{\phi_m} \varphi(\sigma, \Delta/d_m) \tag{8}$$

where ϕ is the volume fraction and $\phi_m = \phi(\Delta = 0)$ is the maximum value of ϕ for a given structure. The function φ (see appendix) in equation (8) is equal to 1 for $\sigma = 0$ and remains very close to 1 for $\sigma < 0.1$. Two systems differing by Δ or σ and characterized by the same value of ϵ_d^{eff} correspond to the same intensity of DDI. Notice that for weak polydispersity, ϵ_d^{eff} is related to the parameter y widely used in the works dealing with the dipolar hard sphere fluid (DHS) which in our notations reads $y = 8\beta^* \phi \epsilon_d/3$.

Although we do not limit our simulations to a specific experimental system, we have in mind iron oxide NP to guide our choice of the physical parameters entering the model. At room temperature the bulk anisotropy constant is K_c =-11.0 to -13.0 kJm^{-3} and -4.70 kJm^{-3} for magnetite and maghemite respectively. The saturation magnetization for these two materials are quite close and lead to $J_s \sim 0.50$T. Therefore in this work we use $J_s = 0.50$ T, which corresponds to $d_{ref} = 10\ nm$ when this later is fixed from $\epsilon_d(d_{ref}) = 1.0$. The shape anisotropy constant can be estimated for ellipsoidal NP once the aspect ratio is known; using $J_s = 0.5T$ we get $K_{sh}^{(u)} \simeq 50(1 - 3N_l)$ kJm^{-3} which leads to $K_{sh}^{(u)} < 7.0$ kJm^{-3} for NP characterized by an aspect ratio $\xi < 1.20$, and accordingly $\epsilon_{uv}^{(0)} = 0.95$. Concerning the surface anisotropy constant, we consider the experimental values ranging from $K_s = 5.5\ 10^{-6}$ Jm^{-2} to $K_s = 2.7\ 10^{-5}$ Jm^{-2} for maghemite[13,22,27]; thus $K_s = 2.7\ 10^{-5}$ Jm^{-2} is considered somewhat as an upper bond for iron oxide NP. Notice that if we consider the deviation from sphericity resulting from a size independent corrugation δ as outlined above, we get $K_{sh}^{(s)} \simeq 2.70\ 10^{-5}$ Jm^{-2} with δ =2 nm, which corresponds to an aspect ratio ranging from 1.4 to 1.2 for NP of diameter ranging from

10 to 20 nm. The corresponding values of the reduced parameters for Iron oxide NP of *c.a.* 10 to 20 nm in diameter are summarized in table I. In the following we can consider that a characteristic value for the uniaxial anisotropy is about $\epsilon_{uv} \sim 5$ while a maximum value for the cubic anisotropy constant is $|k_c| = 15$.

d_m/d_{ref}	1	1.20	1.33	1.71	2.0
ϵ_c [a)]	-1.65	-2.85	-3.88	-8.25	-13.20
ϵ_c [b)]	-0.60	-1.05	-1.41	-3.0	-4.8
ϵ_{uv} [c)]	0.625	1.08	1.47	3.13	5.00
ϵ_{uv} [d)]	1.00	1.73	2.37	5.0	8.00
ϵ_{us} [e)]	2.05	2.95	3.62	6.0	8.20
ϵ_d	1.0	1.73	2.37	5.0	8.00
ϵ_d^{eff} [f)]	0.60	1.09	1.56	3.6	6.00
ϵ_d^{eff} [g)]					1.56

Table I: Reduced values for the parameters of the model corresponding to iron oxide NP. with K_c = - 13 kJm^{-3} [a)] ; -4.7 13 kJm^{-3} [b)]; an aspect ratio $\xi = 1.135$ [c)]; or 1.20 [d)]; or surface anisotropy constant $K_s = 2.70\ 10^{-5}$ Jm^{-2} [e)]. ϵ_d^{eff} from equ. (8) with Δ =2 nm [f)] or 14.5 nm [g)].

The main effect of the DDI on the magnetization curve at low field is a strong reduction of the initial slope of $M(H)$ versus H, namely of the linear susceptibility[36,37]. This is directly related to the well known plateau in the FC magnetization in terms of the temperature for $T < T_B$ occurring in strongly interacting NP and also the the plateau in the $\chi(d_m)$ curve obtained in Ref. [36] for densely packed clusters of NP. Indeed, in the absence of anisotropy, the hamiltonian (6) can be rewritten, with $h_r = H_a/H_{ref}$

$$\beta E = \beta^* \beta_0 E = -\beta^* \epsilon_d^{(0)} \left(\frac{d_m}{d_{ref}}\right)^3 \frac{1}{(1+\Delta/d_m)^3} \sum_{i<j} d_i^{*3} d_j^{*3} \frac{\hat{m}_i \hat{m}_j - 3(\hat{m}_i \hat{r}_{ij})(\hat{m}_j \hat{r}_{ij})}{(r_{ij}^*/(1+\Delta/d_m))^3} - h_r \beta^* \left(\frac{d_m}{d_{ref}}\right)^3 \sum_i d_i^{*3} \hat{m}_i \hat{h} \quad (9)$$

where we have introduced the geometrical sum of the reduced DDI of the most concentrated cluster (Δ =0) of the structure considered, namely where particles can get at contact which thus depends neither on d_m and Δ. Introducing the dimensionless variable

$\lambda = \beta^*(d_m/d_{ref})^3$ we get

$$\beta E = -\lambda\epsilon_d^{eff(0)} \sum_{i<j} d_i^{*3} d_j^{*3} \frac{\hat{m}_i\hat{m}_j - 3(\hat{m}_i\hat{r}_{ij})(\hat{m}_j\hat{r}_{ij})}{(r_{ij}^*/(1+\Delta/d_m))^3} - h_r\lambda \sum_i d_i^{*3}\hat{m}_i\hat{h} \tag{10}$$

From equation (10), we can conclude that, when the field is vanishingly small, the leading contribution to the magnetization linear in h_r depends on h_r and β^* only through λh_r and $\lambda\epsilon_d^{eff(0)}$. More precisely, $M/M_s \simeq \lambda h_r f(\lambda\epsilon_d^{eff(0)})$ with f a scaling function. Thus the linear susceptibility, $\chi = \partial M/\partial H_a \simeq M/H_a$ at vanishing H_a must be in the form

$$\chi = \frac{M_s}{H_{ref}}\lambda f(\lambda\epsilon_d^{eff(0)}) \tag{11}$$

In the limit of zero coupling $f(x=0)$ is a finite constant and we recover the Langevin result, $\chi \propto \lambda = (6/\pi)(T_0/T)v(d_m)$. In the interacting system, the strong coupling limit $\lambda\epsilon_d^{eff(0)} >> 1$ or equivalently $y >> 1$ is obtained through the increase of either the DDI coupling, $\epsilon_d^{(0)}$ or β^* (decrease of T). In this case, the limiting value of the susceptibility can be obtained. We note that the linear susceptibility we deal with is the external one, relating the magnetization to the external, or applied field H_a and since we consider the magnetization per unit magnetic volume, the magnetization per unit volume is $M_v = M\phi$. Thus the internal field is related to the external one through $H_i = H_a - D_h\phi M$ where D_h is the demagnetizing factor of the sample in the direction of the field. Hence we can relate χ to the internal susceptibility, χ_i through the usual way[16]

$$\chi = \frac{\chi_i}{1 + D_h\phi\chi_i} \tag{12}$$

We can also introduce the relative permeability, $\mu = (1 + \phi\chi_i)$ to get

$$\phi\chi = \frac{\mu - 1}{1 + D_h(\mu - 1)} \tag{13}$$

In the case of a spherical system as those considered here, $D_h = 1/3$ and equation (13) reads

$$\phi\chi = \frac{3(\mu - 1)}{\mu + 2} \tag{14}$$

It is worth mentioning that χ is related to the moment fluctuations through the fluctuation-dissipation theorem[40] as already used in [36]. We have in an isotropic system

$$\frac{\partial(M/M_s)}{\partial h} = \chi_r = \beta^* \frac{N\bar{v}}{3v(d_m)} \left(\frac{\left\langle (|\Sigma\vec{m}_i|)^2 \right\rangle}{(\Sigma m_i)^2} - \frac{|\langle\Sigma\vec{m}_i\rangle|^2}{(\Sigma m_i)^2} \right) \equiv \beta^* \frac{\bar{v}\ g}{3v(d_m)} \tag{15}$$

which introduces the factor g and where $\bar{v}$ is the average value of the particle volume over the distribution function. From equation (15) we rewrite (14) in the equivalent form

$$\frac{3(\mu-1)}{\mu+2} = \phi\chi = 8\phi\epsilon_d\beta^* \frac{\bar{v}}{v(d_m)} g \tag{16}$$

Now in the strong coupling limit we expect the system to reach a ferromagnetic transition as is the case for the DHS fluid[38,39]. In this limit the permeability $\mu \to \infty$ and a limiting value for χ and thus a plateau in the FC magnetization when the temperature is decreased is obtained with, from equation (14)

$$\chi \to \frac{3}{\phi} \quad \text{or} \quad \tilde{\chi} \to \frac{3}{8\epsilon_d^{(0)}\phi} \quad \text{with} \quad \tilde{\chi} = \frac{H_{ref}}{M_s}\chi \tag{17}$$

This is quite well reproduced by the present simulations (see section (III)) and in total agreement with the behavior of $\tilde{\chi}$ in terms of the particle size d_m we obtained in Ref. [36] in the quasi monodisperse case where $\varphi \simeq 1$ which is easily deduced from (17) by writing ϕ in terms of Δ/d_m

$$\tilde{\chi} \to \frac{\varphi\ (1+\Delta/d_m)^3}{8\epsilon_d^{(0)}\phi_m} \tag{18}$$

It is important to note that equation (14) is the well known relation between the dielectric constant and the polarization susceptibility in the DHS fluid in the case of an infinite spherical system embedded in vacuum, *i.e.* surrounded by a medium of dielectric constant $\epsilon_s = 1$. Indeed the magnetic permeability plays the role of the dielectric constant of the DHS and the polarization susceptibility is related to the fluctuations or the Kirkwood factor $g_K(\epsilon_s)$, equivalent to the factor g introduced above; in the monodisperse case, with the dielectric constant, ϵ, in place of μ the DHS satisfies[40,41]

$$\frac{\mu-1}{\mu+2} = y g_K(\epsilon_s = 1) \ \ ; \text{ or } \quad \mu - 1 = 3y g_K(\epsilon_s = \infty) \tag{19}$$

Notice that the second equation (19) is the equivalent of (13) written for $D_h = 0$ and corresponds to the case where either through the boundary conditions ($\epsilon_s = \infty$) or the system shape ($D_h = 0$) the system can be uniformly polarized. Equation (19) is strictly equivalent to (16) since in the present model we have, in the monodisperse case, $\chi_r = \beta^* g/3$. The DHS undergoes a ferromagnetic transition at which the dielectric constant diverges and as a result[38,42,43], one expects a limiting value for the Kirkwood factor $g_K(\epsilon_s = 1) \to 1/y$ and accordingly $\chi_r \to \beta^*/(3y)$ or $\chi \to 3/\phi$ in agreement with equation (17).

The plateau in the FC magnetization at low temperature and low field is a behavior observed in the framework of the FC/ZFC procedure[25,29,44–46] generally related to a col-

lective behavior of the dipoles leading to a frozen state. Here, by analogy with the known behavior of the DHS fluid, we relate this plateau to the approach of the onset of the ferromagnetic transition at least for $\sigma << 1$ and in the absence of MAE. We emphasize that as can be deduced from equation (14), in the case of a spherical system surrounded by vacuum, χ becomes nearly independent of μ when μ increases beyond a sufficiently high ($\mu \sim 35$) but still finite value. As a result χ gets close to its limiting value before the ferromagnetic transition.

The Monte Carlo simulations are performed according to the usual Metropolis scheme[40,41,47]. The trial move of each moment is performed within a solid angle centered on its old position. Since we seek equilibrium configurations, the maximum solid angle of the move is only restricted by the acceptance ratio, $R \sim 0.35$–0.50. Moreover we use a annealing scheme at all values of the field in the range where we expect an hysteresis. The averages are performed on 10 to 30 independent runs (up to 70 runs for low temperature and/or large DDi couplings) with $3\,10^4$ to $4\,10^4$ thermalisation MC steps followed by another set of $3\,10^4$ to $4\,10^4$ MC steps to compute the averages.

III. RESULTS

Non interacting system

In this section we deal with the case free of DDI. We first have checked that as $h \to 0$ with volume uniaxial MAE and a random easy axes distribution the linear susceptibility is ϵ_{uv} independent while with cubic MAE and randomly distributed axes, both the linear and the first non linear susceptibilities are k_c independent and accordingly we get a nearly k_c independent M(h) beyond the very vicinity of $h = 0$. This is shown in figure 1 in terms of the inverse reduced temperature β^*. Moreover we also check in figure 1 that the deviation of $M(h)$ relative to the isotropic case is negative whatever the sign of k_c with the random distribution of cubic axes. This is no more the case when the cubic axes of the particles are fixed where on the one hand only the linear susceptibility is k_c independent and on the other hand the sign of $(M(h, k_c) - M(h, k_c = 0))$ depends on the sign of k_c. The same result holds when $\epsilon_d \neq 0$.

For randomly distributed cubic axes, the cubic MAE has only a negligible effect on the $M(h)$ curve. On the opposite, as shown in figure 2, when the cubic axes are fixed along the system frame, the cubic MAE has a strong effect on the $M(h)$ curve. Moreover, as noted above in the low field region, the sign of the anisotropy induced deviation of $M(h)$ depends on the sign of k_c. This is expected since a positive value of k_c will favor the principal frame directions for the moments; for an applied field along one of these

directions, say $\hat{h}=\hat{z}$, $k_c > 0$ leads to a positive deviation of $M(h)$ and *vice versa*. The results displayed in figure 2 are in agreement with those of Ref. [33] (notice that our k_c corresponds to $w/2$ of Ref. [33]).

The effect of the texturation through the preferential orientation along the $\hat{z}$-axis of the crystallites [111] direction according to the probability density (4) is shown in figure 3 for the polydisperse and monodisperse cases.

Concerning the uniaxial anisotropy, we note that the surface contribution can be very well approached by the volume term with the introduction of an effective volume uniaxial constant, ϵ_{uv}^{eff} taking into account the polydispersity. In equation (6), we rewrite the uniaxial energy terms by introducing the reduced $n-th$ order moments d_n^* of the diameter distribution function and under the hypothesis that $(\sum d_i^{*n}(\hat{n}_i\hat{m}_i)^2)/d_n^*$ is independent of n at least for $n \leq 3$ we get

$$\epsilon_{uv}^{eff} = \frac{d_2^*}{d_3^*}\epsilon_{us} = \exp(-5\sigma^2/2)\epsilon_{us} \tag{20}$$

where we have used the analytical result for the d_n^* of the lognormal law. The same conclusion holds in presence of DDI; in figure 4 we compare the deviation of $M(h)$ due to the surface uniaxial MAE with that due to the volume uniaxial MAE with $\epsilon_{uv} = \epsilon_{uv}^{eff}$ taken from (20) in the case of a polydisperse interacting system.

We now consider the case of combined uniaxial and cubic anisotropies. The result is shown for a typical set of parameters, $\epsilon_{uv} = 5$ and $|k_c| = 15$ in figure 5. As is the case when only the cubic anisotropy is taken into account, we find that the effect on $M(h)$ of the cubic anisotropy with random distributed cubic axes is very small when the uniaxial easy axes are also randomly distributed and uncorrelated from the cubic ones. This is no more the case when, still for a random distribution of cubic axes, the easy axes $\{\hat{n}\}_i$ are along a specified crystallographic orientation of the crystallites. The cubic MAE enhances the uniaxial one when $\epsilon_c > 0$ and $\{\hat{n}\}_i = [001]$, or when $\epsilon_c < 0$ and $\{\hat{n}\}_i = [111]$. This is qualitatively expected since then the two components of the MAE tend to favor the same local orientation for the moment.

A shoulder in $M(h)$ is clearly observed when $\{\hat{n}\}_i = [001]$ and $\epsilon_c > 0$ or $\{\hat{n}\}_i = [111]$ and $\epsilon_c < 0$. This can be compared to the behavior of the hysteresis curves determined by Usov and Barandiarán [32] when the easy axis of the uniaxial MAE component is fixed relative to the NP frame. This shoulder is enhanced when either the inverse temperature β increases or when the polydispersity σ increases (see figure 6). This latter point is simply due to the presence of larger particles in the distribution when σ increases, with accordingly larger anisotropy energies. We can be interpret this feature as the coherent contributions of uniaxial and cubic terms. In the case $\epsilon_c < 0$ where the favorable orientations are the

{111} axes, we find that the cubic contribution remains to enhance the uniaxial anisotropy constant by a factor of roughly $|\epsilon_c|/5$ as shown in the inset of figure (5).

Interacting systems

Most of our simulations with DDI are performed with free boundary conditions (FBC) on large spherical NP clusters of $N_p \sim 1000$ particles. In order to check the validity of the method, we have performed simulations with periodic boundary conditions (PBC) with Ewald sums for the DDI in both the conducting or the vacuum external boundary conditions[40,41]. This is done by using either ϵ_s=1 or $\epsilon_s = \infty$ for the surrounding permeability (or dielectric constant in the electric dipolar case). Here we are interested in the determination of the linear susceptibility for the infinite system embedded in vacuum, as we seek the magnetic response in terms of the external field. Therefore, we check that one can get $\chi_r(\epsilon_s = 1)$ from simulations on a large spherical NP cluster with FBC, or by using PBC with Ewald sums in either the conducting or the vacuum boundary conditions. The value of $\chi_r(\epsilon_s = 1)$ can be obtained from a simulation with external conducting conditions by exploiting in equation (19) the independence of μ with respect of ϵ_s as it is an intrinsic property ,

$$\chi_r(\epsilon_s = 1) = \chi_r(\epsilon_s = \infty)/(1 + 8\phi\epsilon_d\chi_r(\epsilon_s = \infty)). \tag{21}$$

The comparison of $\chi_r(\epsilon_s = 1)$ from the three routes is shown in figure 7 in the absence of anisotropy and in the quasi monodisperse case ($\sigma = 0.05$). We have used the same initial cluster and extracted either a spherical cluster for FBC or a cubic simulation box for PBC with a value of Δ fitted on the volume fraction ϕ. Moreover we have checked that for moderate values of the DDI coupling the permeability obtained from these three routes leads to similar values. These two points show the coherence of our simulations with DDI. When compared to the results of Klapp and Patey [48] the curve $\mu(y)$ we get at $\phi = 0.385$ lies in between the ones of the frozen model with correlation and of the frozen model with quenched disorder, much closer to the former and in fact very close to that of the DHS fluid.

Beside the strong reduction of the initial susceptibility, the DDI reduce also the deviation of the $M(h)$ curves due to MAE, as can be seen in figure 8. As expected the cubic anisotropy has nearly no influence on the $M(h)$ when the easy axes and the cubic axes are independently randomly distributed; on the other hand the change in the $M(h)$ curve due to the cubic contribution when $\{\hat{n}\}_i$ are along the crystallites [111] with $k_c < 0$ or along the [001] with $k_c > 0$ is smaller than in the absence of DDI. Nevertheless, the contribution

of the cubic anisotropy may be not negligible under the condition of a coherence with the uniaxial term. Moreover, we do find that in order for the cubic term to give a noticeable effect a rather large value of the cubic anisotropy constant, k_c is necessary.

In opposite to what we get in the absence of DDI, we do not find any distinctive feature of either the cubic or the uniaxial symmetry on the $M(h)$ curve if the cubic axes are randomly distributed in the case of combined or only uniaxial anisotropy. This is shown in figure 9 where different combinations of anisotropies leading to comparable $M(h)$ curves are considered for $\epsilon_d^{eff} = 1$.

Finally we consider the comparison with the experimental magnetization curves of Ref. [49] on powder samples of maghemite NP differing by their size. These samples are characterized by a polydispersity $\sigma \sim 0.27$ and the estimated coating layer thickness is *c.a.* 2 nm. The behavior of the $M(H_a)$ curve being controlled by the DDI and the MAE at low and intermediate values of the applied field respectively, we fit the value of Δ by the slope at $H_a \sim 0$ and the anisotropy constants on the behavior of $M(H_a)$ at higher values of H_a. We find that the region $H_a \sim 0$ is well reproduced with $\Delta = 2\ nm$ for $d_m = 10\ nm$ and 21 nm, and $\Delta = 2.4\ nm$ for 12 nm, which does not differ much from the estimated experimental value. Concerning the cubic anisotropy since the experimental samples are not textured we consider only a random distribution of cubic axes. The value of the corresponding anisotropy constant may differ from its known bulk value due to surface effects; however, we consider the bulk value as a starting point. In any case, since the cubic anisotropy constant for iron oxide is rather small, we expect only a small effect of the cubic contribution to the MAE and accordingly we consider only the case where the cubic and the uniaxial components of the MAE reinforce each other. With $\epsilon_c < 0$, this means that we limit ourselves to a easy axes distribution $\{\hat{n}\}_i = [111]_i$. For the uniaxial MAE we have to choose either a surface or volume dependent MAE (see equation (6)); however, we have shown that the surface dependent MAE can be reproduced by the volume dependent one through the effective constant of (20). Hence, starting from the bulk value for ϵ_c we are left with ϵ_{uv} as the only fitting parameter. We find $\epsilon_{uv} = 4.00$ for $d_m = 10\,nm$ by fitting $M(H_a)$ in the intermediate field range; then, the same quality of agreement between the model and the experimental curves is obtained for $d_m = 12\,nm$ and $21\,nm$ by using a value of ϵ_{uv} scaling as d_m^3, namely $\epsilon_{uv} = 6.912$ and 32.0 for $d_m/d_{ref} = 1.2$ and 2.0 respectively, *i.e.* $K_v = 31.6$ kJm^{-3} (we use the simulated curve for $d_m/d_{ref} = 2$ for comparison of the experimental curves of the samples with d_m 18 and 21 nm; only the second is presented here). Notice the weak hysteresis cycle for the experimental sample characterized by $d_m = 21$nm; this is due to the largest particles in the distribution and is not reproduced by the M.C. simulations, since we have chosen to perform equilibrium ($\tau_m = \infty$) simulations only. The cubic MAE gives only a small contribution to $M(H_a)$

as illustrated by the difference obtained using ϵ_c deduced from either the magnetite or the maghemite bulk values given in Table I (see figures 11 and 12). Therefore, we find that using the iron oxide bulk value for the cubic MAE constant the experimental NP of Ref. [49] can be modeled excepted in the high field region, by NP presenting a volume dependent uniaxial anisotropy with $K_v = 31.6\,\mathrm{kJm^{-3}}$. However, as we have shown, we can get similar $M(H_a)$ curves with different combinations of cubic and uniaxial MAE especially with the DDI which weaken the peculiar features of the cubic contribution. Hence, we can get the same agreement with experiment by using on the one hand a uniaxial MAE scaling as d_m^2 corresponding to a surface anisotropy and on the other hand a fitted cubic contribution. Starting from $\epsilon_{uv} = 4$ for $d_m/d_{ref} = 1.0$ this gives $\epsilon_{uv} = 5.76$ for dm/d_{ref} 1.2 (which translates to $\epsilon_{us} = 7.03$ for $\sigma = 0.28$ and $K_s = 6.45\,10^{-5}$ $\mathrm{Jm^{-2}}$). The corresponding cubic component is obtained from our finding that an increase of $|\epsilon_c|$ corresponds to an increase of ϵ_{uv} of roughly $|\epsilon_c|/5$, leading to ϵ_c = -9 and K_c = -41 $\mathrm{kJm^{-3}}$. We have also considered a fitted cubic MAE with a positive ϵ_c, and $\hat{n}_i = [001]_i$ for which we find $\epsilon_c = 5.0 (K_c = 25.15\ \mathrm{kJm^{-3}})$. The results is shown in figure 11. Doing this means that the cubic anisotropy energy present an anomalous component, namely $\left|K_c - K_c^{bulk}\right|$, scaling as the NP volume while it should be understood as a surface effect. Hence, although it seems difficult to conclude on the best fit of the experimental set considered, it may be better to avoid the latter contradiction and consider these NP as presenting a volume dependent uniaxial MAE; however, we then get a value for the effective anisotropy constant too large to be explained only as a shape anisotropy. It is nevertheless still in the range of what is obtained experimentally from T_B for iron oxide NP. In any case, we have to take such conclusions with care given the simplicity of the model. Similarly, the high field range cannot be reproduced with the simple OSP model and necessitates a the inclusion of a field dependent description of the individual NP.

IV. CONCLUSION

In this work, we have performed Monte Carlo simulations of room temperature magnetization curves in the superparamagnetic regime, with a particular attention paid to the iron oxide based NP. We focused on the search for a peculiar feature of the cubic MAE component on the $M(H_a)$ curve since iron oxide and spinel ferrites in general presents an intrinsic MAE with cubic symmetry while from experiments a uniaxial MAE is generally found. Our result is that a peculiar feature of the cubic component can be obtained only *i)* if the the cubic and the uniaxial components are correlated through the alignment of the NP easy axes on a specified crystallographic orientation of the crystallites; *ii)* if the DDI are negligible *via* a small NP volume fraction. Nevertheless a large value of the cubic

MAE constant compared the uniaxial one is necessary for the former to give a noticeable effect on the room temperature $M(H_a)$.

V. APPENDIX A

In this appendix we explicit the function φ introduced in equation (8). The volume fraction is defined as

$$\phi = N_p \frac{1}{V} \int_0^\infty f(d) \frac{\pi}{6} d^3 d(d) = \frac{\pi d_m^3}{6V} d_3^* \tag{A.1}$$

where V is the total volume and d_n^* is the reduced $n-th$ moment of $f(d)$. Each particle of diameter d is surrounded by a coating layer of thickness $\Delta/2$; the maximum value of the volume fraction, ϕ_m is obtained as the volume fraction of the spheres including both the particles and the coating layer, namely by replacing d in (A.1) by $(d + \Delta)$ with the same distribution function. Defining $\Delta^* = \Delta/d_m$ we get

$$\begin{aligned} \phi_m &= N_p \frac{1}{V} \int_0^\infty f(d) \frac{\pi}{6} (d+\Delta)^3 d(d) \\ &= \frac{\pi d_m^3}{6V} d_3^* (1+\Delta^*)^3 \left[\frac{1 + 3\Delta^* (d_2^*/d_3^*) + 3\Delta^{*2} (d_1^*/d_3^*) + \Delta^{*3} (1/d_3^*)}{(1+\Delta^*)^3} \right] \end{aligned} \tag{A.2}$$

which defines the function φ as the expression in square brackets. From the analytical expression of the reduced moments d_n^* in the lognormal law, $d_n^* = \exp(n^2\sigma^2/2)$ we get

$$\varphi = \left[\frac{1 + 3\Delta^* e^{-5\sigma^2/2} + 3\Delta^{*2} e^{-4\sigma^2} + \Delta^{*3} e^{-9\sigma^2/2}}{(1+\Delta^*)^3} \right] \tag{A.3}$$

Acknowledgments

This work was granted access to the HPC resources of CINES under the allocation 2013-c096180 made by GENCI (Grand Equipement National de Calcul Intensif).

[1] R. Skomski, J. Phys.: Condens. Matter **15**, R841 (2003).

[2] X. Battle and A. Labarta, J. Phys D **35**, R15 (2002).

[3] S. Bedanta and W. Kleemann, J. Phys D **42**, 013001 (2009).

[4] S. Majetich and M. Sachan, J. Phys D **39**, R407 (2006).

[5] S. Bader, Review of Modern physics **78**, 1 (2006).

[6] Q. Pankhurst, J. Connolly, S. Jones, and J. Dobson, J. Phys D **36**, R167 (2003).

[7] A. K. Gupta and M. Gupta, Biomaterials **26**, 3995 (2005).

[8] R. H. Kodama, A. E. Berkowitz, E. J. McNiff, Jr., and S. Foner, Phys. Rev. Lett. **77**, 394 (1996).

[9] Y. Labaye, O. Crisan, L. Berger, J. M. Greneche, and J. M. D. Coey, Journal of Applied Physics **91**, 8715 (2002).

[10] L. Berger, Y. Labaye, M. Tamine, and J. M. D. Coey, Phys. Rev. B **77**, 104431 (2008).

[11] V. Russier, Journal of Applied Physics **105**, 073915 (2009).

[12] M. P. Morales, S. Veintemillas-Verdaguer, M. I. Montero, C. J. S erna, A. Roig, L. Casas, B. Martínez, and F. Sandiumenge, Chemistry of Materials **11**, 3058 (1999).

[13] E. Tronc, D. Fiorani, M. Noguès, A. Testa, F. Lucari, F. D'Orazio, J. Grenèche, W. Wernsdorfer, N. Galvez, C. Chanéac, et al., Journal of Magnetism and Magnetic Materials **262**, 6 (2003).

[14] D. A. Garanin and H. Kachkachi, Phys. Rev. Lett. **90**, 065504 (2003).

[15] H. Kachkachi and E. Bonet, Phys. Rev. B **73**, 224402 (2006).

[16] J. M. D. Coey, *Magnetism and Magnetic Materials* (Cambridge University Press, 2010).

[17] J. B. Birks, Proc. Phys. Soc. B **63**, 65 (1950).

[18] L. R. Bickford, Phys. Rev. **78**, 449 (1950).

[19] E. Babkin, K. Koval, and V. Pynko, Thin Solid Films **117**, 217 (1984).

[20] W. H. P. Smit J., *Physical properties of ferrimagnetic oxides in relation to their technical applications* (Philips Technical Library, 1959).

[21] L. Néel, J. Phys. Radium **15**, 255 (1954).

[22] F. Gazeau, J. Bacri, F. Gendron, R. Perzynski, Y. Raikher, V. Stepanov, and E. Dubois, Journal of Magnetism and Magnetic Materials **186**, 175 (1998).

[23] A. G. Roca, M. P. Morales, K. O'Grady, and C. J. Serna, Nanotechnology **17**, 2783 (2006).

[24] P. Dutta, A. Manivannan, M. S. Seehra, N. Shah, and G. P. Huffman, Phys. Rev. B **70**, 174428 (2004).

[25] K. Nadeem, H. Krenn, T. Traussnig, R. Würschum, D. Szabó, and I. Letofsky-Papst, Journal of Magnetism and Magnetic Materials **323**, 1998 (2011).

[26] A. Demortiere, P. Panissod, B. P. Pichon, G. Pourroy, D. Guillon, B. Donnio, and S. Begin-Colin, Nanoscale **3**, 225 (2011).

[27] M. Tadić, V. Kusigerski, D. Marković, M. Panjan, I. Milošević, and V. Spasojević, Journal of Alloys and Compounds **525**, 28 (2012).

[28] C. Pereira, A. M. Pereira, P. Quaresma, P. B. Tavares, E. Pereira, J. P. Araujo, and C. Freire, Dalton Trans. **39**, 2842 (2010).

[29] C. Pereira, A. M. Pereira, C. Fernandes, M. Rocha, R. Mendes, M. P. Fernández-García, A. Guedes, P. B. Tavares, J.-M. Grenèche, J. P. Araújo, et al., Chemistry of Materials **24**, 1496 (2012).

[30] R. Skomski, *Simple models of magnetism* (Oxford University Press, 2008).

[31] J. García-Palacios, *Advances in Chemical Physics* (John Wiley and Sons, Inc., 2000), vol. 112,

pp. 1–210.

[32] N. A. Usov and J. M. Barandiarán, Journal of Applied Physics **112**, 053915 (2012).

[33] G. Margaris, K. Trohidou, and H. Kachkachi, Phys. Rev. B **85**, 024419 (2012).

[34] Y. Lalatonne, L. Motte, J. Richardi, and M. P. Pileni, Phys. Rev. E **71**, 011404 (2005).

[35] E. du Trémolet de Lacheisserie, *Magnétisme* (EDP Sciences, 2000), in french.

[36] V. Russier, C. de Montferrand, Y. Lalatonne, and L. Motte, Journal of Applied Physics **112**, 073926 (2012).

[37] R. W. Chantrell, N. Walmsley, J. Gore, and M. Maylin, Phys. Rev. B **63**, 024410 (2000).

[38] J. J. Weis and D. Levesque, Phys. Rev. E **48**, 3728 (1993).

[39] D. Wei and P. G.N., Phys. Rev. Lett. **68**, 2043 (1992).

[40] M. P. Allen and D. J. Tildesley, *Computer Simulation of Liquids* (Oxford Science Publications, 1987).

[41] D. Frenkel and B. Smit, *Understanding molecular simulations* (Academic Press, 2002).

[42] J.-J. Weis, The Journal of Chemical Physics **123**, 044503 (2005).

[43] J.-J. Weis and D. Levesque, The Journal of Chemical Physics **125**, 034504 (2006).

[44] J. M. Vargas, W. C. Nunes, L. M. Socolovsky, M. Knobel, and D. Zanchet, Phys. Rev. B **72**, 184428 (2005).

[45] D. Caruntu, G. Caruntu, and C. J. O'Connor, Journal of Physics D: Applied Physics **40**, 5801 (2007).

[46] Y. Tan, Z. Zhuang, Q. Peng, and Y. Li, Chemistry of Materials **20**, 5029 (2008).

[47] K. Binder and D. W. Heerman, *Monte Carlo Simulation in Statistical Physics* (Springer, 1997).

[48] S. H. L. Klapp and G. N. Patey, The Journal of Chemical Physics **115**, 4718 (2001).

[49] C. de Montferrand, Y. Lalatonne, D. Bonnin, N. Lièvre, M. Lecouvey, P. Monod, V. Russier, and L. Motte, Small **8**, 1945 (2012).

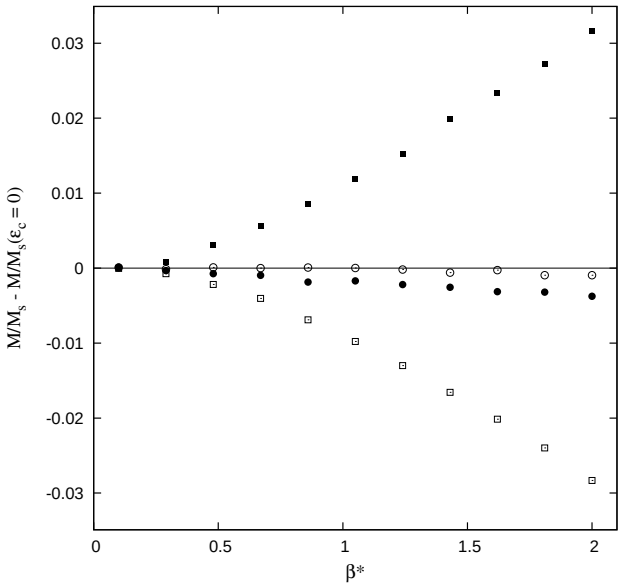


Figure 1: Deviation of the reduced magnetization M/M_s due to MAE at $h = 0.20$ for a non interacting system with cubic anisotropy. Polydispersity: $\sigma = 0.28$. Cubic axes randomly distributed and ϵ_c =15, solid circles; ϵ_c = -15, open circles. Cubic axes fixed and parallel to the system frame with $\epsilon_c = 15$, solid squares; ϵ_c = -15, open squares.

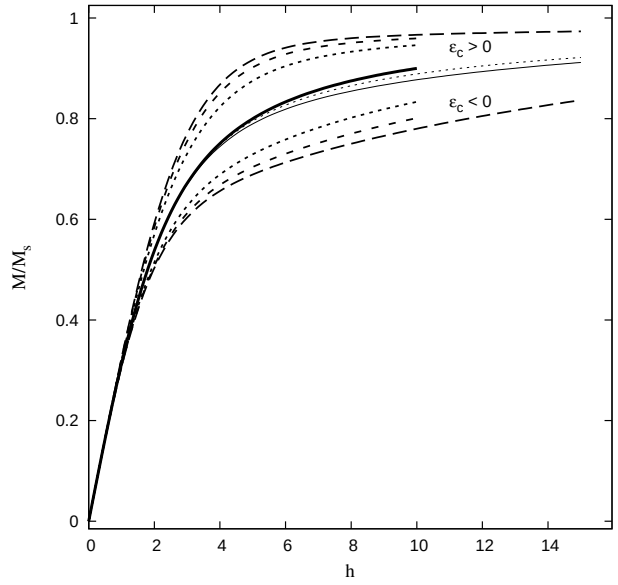


Figure 2: Magnetization curve for a monodisperse non interacting system with cubic anisotropy. The cubic anisotropy axes are fixed along the system frame with $\epsilon_c = \pm$ 15 long dashed; $\pm$ 12 dashed; and $\pm$ 8 short dasched. The sign of ϵ_c is as indicated. The case with random distribution of the cubic axes is shown for comparison with $\epsilon_c = 15$, thin solid line; and ϵ_c =-15, thin dotted line. The thick solid line is the reference $\epsilon_c = 0$ case. $\beta^* = 1$.

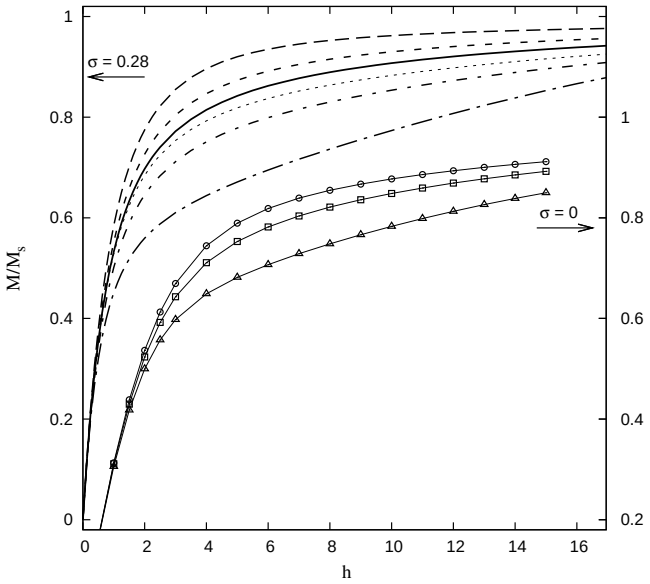


Figure 3: Magnetization curve for non interacting system with cubic anisotropy, $|\epsilon_c| = 15$ and $\beta^* = 1$. The [111] direction of the cristallites are prefentially oriented along the z axis (which is also the direction of the field) with the probability distribution of equation (4). Polydisperse case ($\sigma = 0.28$) with ϵ_c = -15 and $\sigma_\theta = 0.015$, long dash; $\pi/10$, short dash; $\pi/2$, solid line. Same with $\epsilon_c = 15$ and $\sigma_\theta = \pi/2$, dotted line; $\pi/10$, short dash dot; 0.015, long dash dot. Monodisperse case ($\sigma = 0$) with $\epsilon_c = 15$ and $\sigma_\theta = 0.015$, open triangles; $\pi/10$, open squares; $\pi/2$, open circles.

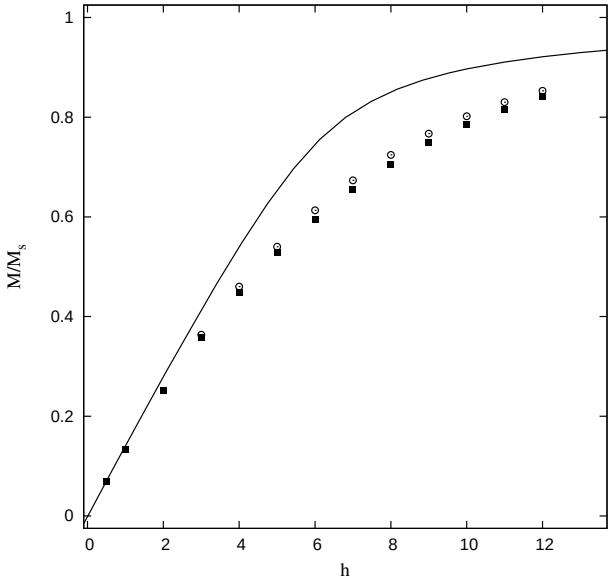


Figure 4: M(h) for an interacting system characterized by $\epsilon_d = 2.37$, $\Delta/d_{ref} = 0.20$, $d_m/dref = 1.33$ and $\beta^* = 1$. Without anisotropy: solid line. In the presence of uniaxial anisotropy with $\epsilon_{uv} = 5.64$ and $\epsilon_{us} = 0.0$, solid squares; $\epsilon_{uv} = 0.0$ and $\epsilon_{us} = 6.88$, open circles. (The value $\epsilon_{us} = 6.88$ corresponds to $\epsilon_{uv}(d_3^*(\sigma)/d_2^*(\sigma))$ with $\epsilon_{uv} = 5.64$, d_n^* is the n-th moment of the diameter distribution function.)

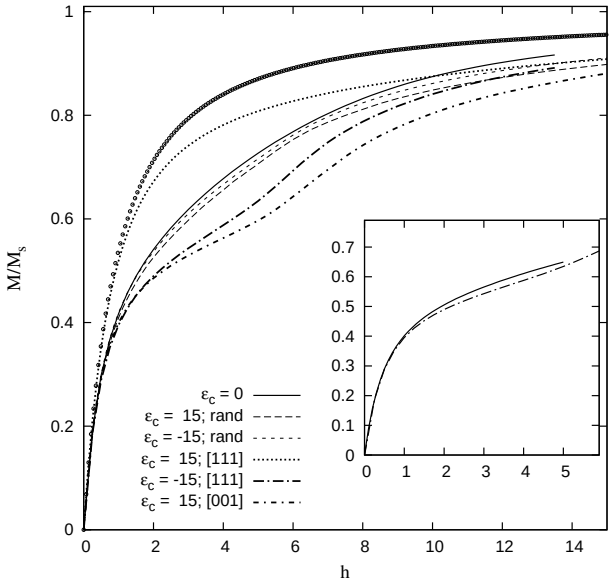


Figure 5: Magnetization curve for non interacting system with uniaxial and cubic anisotropies with $\beta^* = 1$, $\epsilon_{uv} = 5$, $\epsilon_{us} = 0$ and $|\epsilon_c| = 15$. Polydispersity : $\sigma = 0.28$. Open circles: case free of anisotropy for comparison. ϵ_c and easy axes distributions as indicated. Inset : comparison of the $M(h)$ curves for $\epsilon_{uv} = 5$ and $\epsilon_c = -15$, long dash dotted line and for $\epsilon_{uv} = 8$ and $\epsilon_c = 0$, solid line.

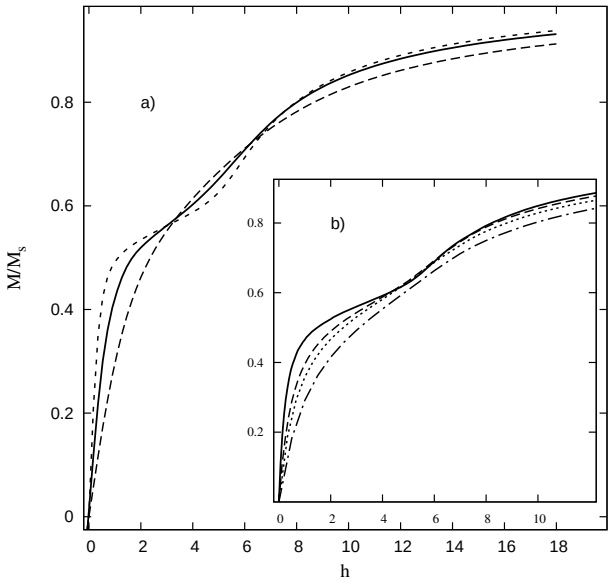


Figure 6: Reduced magnetization for a non interacting system with $\epsilon_{uv} = 5.0$, ϵ_c = -15, cubic axes randomly distributed, easy axes along the [111] NP cristallographic orientations and different values of the reduced inverse temperature β^*. $\beta^* = 0.5$, dash dotted line; 0.75, dotted line; 1.0, long dashed line; 2.0, solid line; 4.0 short dashed line. *a)* monodisperse system ($\sigma = 0$); *b)* polydispersity $\sigma = 0.28$.

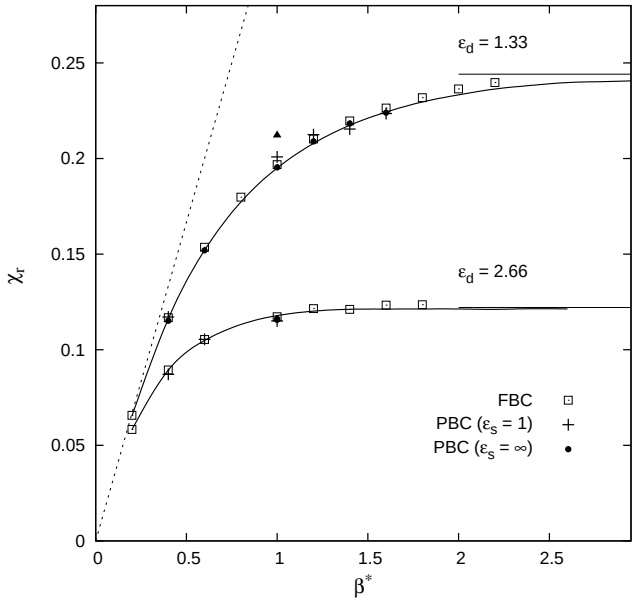


Figure 7: Reduced linear susceptibility, χ_r versus the inverse reduced temperature β^* in the quasi modisperse case, $\sigma = 0.05$ for a volumic fraction $\phi = 0.385$, $\epsilon_d = 1.33$ and 2.66 ($\epsilon_d^{eff} = 1.0$ and 2.0 respectively). Different boundary conditions are considered. In the PBC with Ewald sums, the number of particles is $N_p = 600$ while the clusters for the FBC include $N_p = 1000$ particles. Solid line : M/M_s for $h = 1$. Solid horizontal lines indicate the limit for $y \rightarrow \infty$, (equation (17). The solid triangle at $\beta^* = 1$ indicates the value of χ_r for $\epsilon_d^{eff} = 1.0$ in the polydisperse case $\sigma = 0.28$ ($\epsilon_d = 1.73$; $\Delta/r_m = 0.40$).

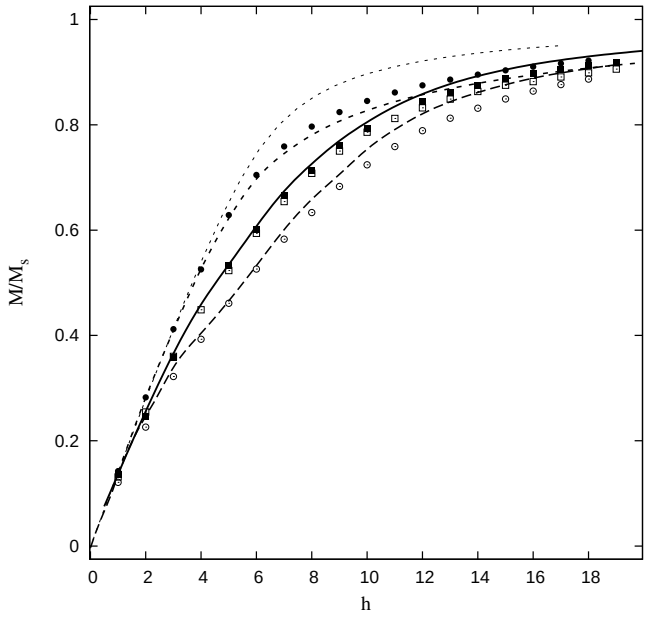


Figure 8: Reduced magnetization for a polydisperse interacting system with $\beta^* = 1$, $\epsilon_d = 2.37$, $\Delta/d_m = 0.15$, polydispersity $\sigma = 0.28$ and different sets of MAE constants. $\epsilon_{uv} = 0.0$ and $\epsilon_c = 0$, dotted line; $\epsilon_{uv} = 5.0$ and $\epsilon_c = 0$, solid line; $\epsilon_{uv} = 5.0$, $\epsilon_c = 15$ and $\hat{n}$ = random, open squares; $\epsilon_{uv} = 5.0$, ϵ_c = -15 and $\hat{n}$ = random, solid squares; $\epsilon_{uv} = 5.0$, $\epsilon_c = 15$ and $\hat{n} = [111]$, short dashed line; $\epsilon_{uv} = 5.0$, ϵ_c = -15 and $\hat{n} = [111]$, long dashed line; $\epsilon_{uv} = 5.0$, ϵ_c = -15 and $\hat{n} = [001]$, solid circles; $\epsilon_{uv} = 5.0$, $\epsilon_c = 15$ and $\hat{n} = [001]$, open circles.

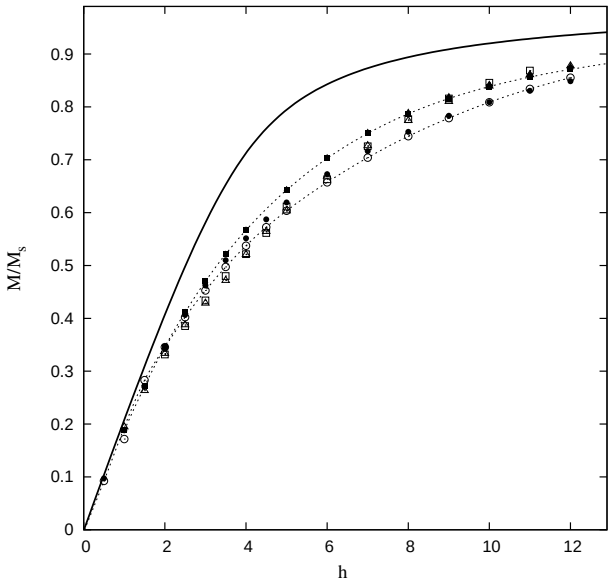


Figure 9: Reduced magnetization for the effective DDI coupling constant $\epsilon_d^{eff} = 1.0$, $\beta^* = 1$, polydispersity $\sigma = 0.28$, open symbols or $\sigma = 0.05$, solid symbols. $\epsilon_{uv} = 6.30$ and $\epsilon_c = 0$, circles; $\epsilon_{uv} = 4.0$, ϵ_c = -12.0 and $\hat{n} = [111]$, squares; $\epsilon_{uv} = 4.0$, $\epsilon_c = 50$, and $\hat{n} = [001]$, triangles. $\epsilon_{uv} = 0.0$, $\epsilon_c = 0$ and $\sigma = 0.28$, solid line. The dotted lines are guides to the eyes.

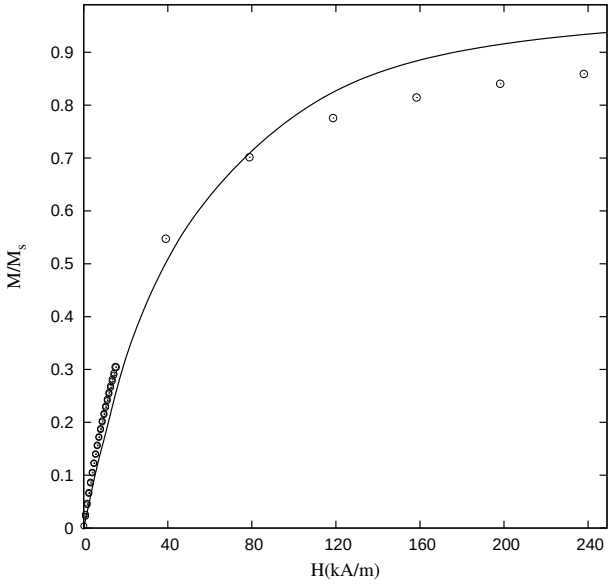


Figure 10: Comparison of the experimental reduced magnetization curve of a maghemite powder sample[49] with $d_m = 10\ nm$, open circles with the M.C. simulation, solid line. The parameters used in the MC simulation are $\sigma = 0.28$, $\epsilon_d = 1.0$, $\Delta/d_m = 0.20$, $\epsilon_{uv} = 4.0$ and $\epsilon_c = -1.5$ with $\hat{n}_i = [111]$. $\beta^* = 1$.

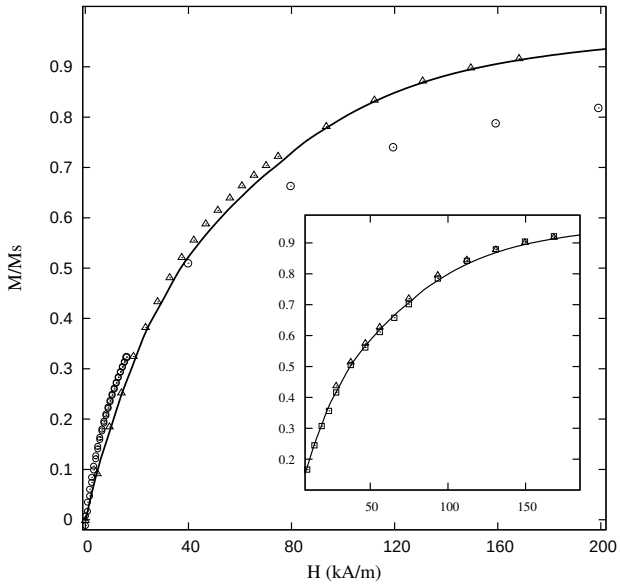


Figure 11: Same as figure 10 for $d_m = 12\ nm$. Experiments[49], open circles. The M.C. simulations are performed with $\sigma = 0.28$, $\epsilon_d = 1.733$, $\Delta/d_m = 0.20$ and different sets of MAE parameters. $\epsilon_{uv} = 6.912$, $\epsilon_c = -2.85$ and $\hat{n}_i = [111]$, solid line. $\epsilon_{uv} = 6.912$, $\epsilon_c = -1.1$ and $\hat{n}_i = [111]$, open triangles. Inset: Comparison of the simulated $M(H_a)/M_s$ curves with $\epsilon_{uv} = 6.912$, $\hat{n}_i = [111]$ and $\epsilon_c = -2.85$, solid line; $\epsilon_{uv} = 5.76$, $\hat{n}_i = [111]$ and $\epsilon_c = -9.00$, open triangles; $\epsilon_{uv} = 5.76$, $\hat{n}_i = [001]$ and $\epsilon_c = 5.50$, open squares.

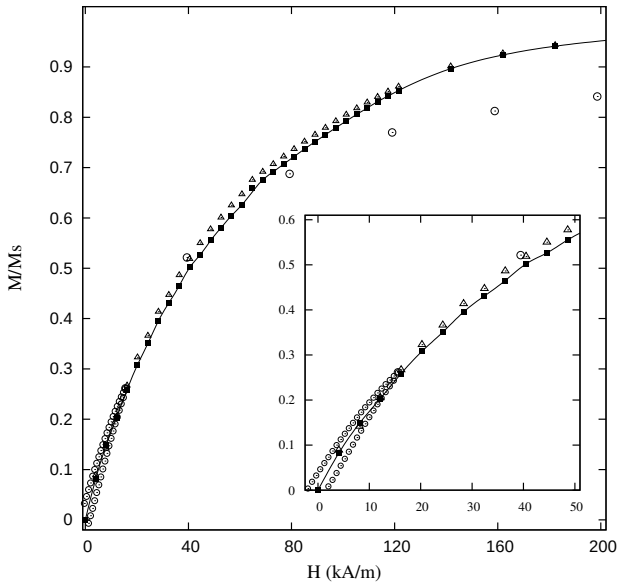


Figure 12: Same as figure 10 for $d_m = 21\ nm$. Experiments[49], open circles. The M.C. simulations are performed with $d_m/d_{ref} = 2$, $\sigma = 0.28$, $\epsilon_d = 8.0$, $\Delta/d_m = 0.10$, $\epsilon_{uv} = 32.00$, $\hat{n}_i = [111]$ and ϵ_c = -13.2, solid squares or ϵ_c = -5.0, open triangles. The thin solid line is a guide to the eyes.